Microphysical interpretation of the seasonal and diurnal variability of the spectral dependence of the aerosol extinction coefficient measured along the near-ground paths

R.F. Rakhimov, V.N. Uzhegov, E.V. Makienko, and Yu.A. Pkhalagov

Institute of Atmospheric Optics, Siberian Branch of the Russian Academy of Sciences, Tomsk

Received December 30, 2003

The array of data on aerosol extinction coefficient $\beta_\varepsilon(\lambda)$ measured along the near-ground path in the wavelength region of 0.44–3.9 μm has been compiled. This data set is used to retrieve size spectra of atmospheric haze and to analyze the effects of random and regular geophysical factors on the seasonal and diurnal variability of the particle size distribution. The microphysical parameters of the haze were determined through direct modeling of the ensembles of realizations of the aerosol extinction coefficient $\beta_\varepsilon(\lambda)$, whose statistical variability ensured the closeness of the eigenvectors of the autocorrelation matrix $\rho_{\beta,\beta}(\lambda_k, \lambda_l)$ to those measured under different weather conditions. The factors have been revealed that determine the diurnal behavior of variations in the size fractions of the near-ground haze. Similar factors have been revealed for the transient period between summer and fall. It has been shown that the peculiarity of the spectral behavior of the aerosol extinction coefficients under different weather conditions is a result of characteristic changes in the number of particles falling within three ranges on the size scale: the accumulative fraction ($r < 0.45$ μm), intermediate fraction ($0.45 < r < 2.0$ μm), and the coarse one ($r > 2.2$ μm).

Introduction

The adequate data on the efficiency of extinction, scattering, and absorption of light by aerosol in a wide wavelength range and different climatic zones are necessary for analysis of the processes determining the transfer of radiation fluxes through the atmosphere (solar radiation with maximum in the visible wavelength range and outgoing IR radiation). These data can be obtained either from empiric optical models of the aerosol atmosphere constructed on the basis of long-term statistically valid measurements of the transmittance spectra of the atmosphere[1,2] or from the so-called models of microphysical imitation of the aerosol light-scattering parameters.[3]

Main advantages of the empiric optical models lie in adequate presentation of the actual atmospheric optical situations. The disadvantage is that such models are constructed for only few geographical regions (center of European part of Russia, Black Sea coast, Kazakhstan arid zone, and south of the Western Siberia).[4–6] Besides, such models describe the spectral coefficients of only aerosol extinction and contain no input parameters characterizing the light absorption by aerosols. At the same time, the models of microphysical imitation of aerosol light scattering free of disadvantages of empiric approach, in their turn, are burdened by specific imperfection due to stylization of the initial data on the aerosol microstructure used.

One of the purposes of this paper is to examine new approach to construction of aerosol models, which combines the advantages of empiric and theoretical methods.

As shown earlier,[7] based on a comparison of experimental data with the results obtained by modeling the statistical variability of the aerosol light-scattering parameters, the correlated changes of the size spectrum and the refractive index of particles under the effect of regular and random variations of the relative air humidity make a basis for the empiric model used for estimating the aerosol scattering phase function by the value of the scattering coefficient. Analogous approach to investigation of the peculiarities of atmospheric variability of the near-ground haze is used in the present paper.

Experimental data

In our study we used the array of data on the aerosol extinction coefficients $\beta_\varepsilon(\lambda)$ at $\lambda = 0.44$, 0.48, 0.52, 0.55, 0.63, 0.69, 0.87, 1.06, 1.25, 1.60, 2.17 and 3.9 μm wavelengths obtained from measurements of the atmospheric transmission spectra $T(\lambda)$ along a 830-m long path in the outskirts of Tomsk. The measurements have been carried out using the instrumentation complex described in Ref. 8. Let us note that the coefficients $\beta_\varepsilon(\lambda)$ were isolated from the total extinction using the statistical method[9] based on multiple linear regression analysis. Measurements covered the period since May 15 until November 4, 2002 and were carried out round-the-clock every two hours. More than 1300 individual realizations of the spectral dependences of the aerosol extinction coefficient $\beta_\varepsilon(\lambda)$ and simultaneously measured values of temperature (t), absolute (a) and relative (q) humidity of the air were obtained.

0235-6880/04/05–06 339-18 $02.00

The mean values and the rms deviations of the coefficients $\beta_\varepsilon(\lambda)$, parameters t, a and q, and those of the calculated components of the aerosol extinction $\Delta\beta_{ac}$, $\Delta\beta_{id}$ and $\Delta\beta_c$ caused by the variability of accumulative ($r \sim 0.05$–0.45 μm), intermediate ($r \sim 0.45$–2.0 μm), and coarse ($r > 2.2$ μm) fractions of the atmospheric haze for the whole data array are shown in Table 1. The correlation coefficients between all these parameters are also presented here. The mean values and the rms deviations of the $\Delta\beta_{ac}$, $\Delta\beta_{id}$ and $\Delta\beta_c$ and of the t, a, and q parameters for each season are presented in Table 2, and their correlations are estimated.

Table 1. Mean values ($\overline{X}$), rms deviations (σ_X) and correlation coefficients ($\rho_{x,x}$) for the entire array of optical-meteorological data obtained since May until November 2002. The array comprises 1351 realizations

Parameters	$\overline{X}$	σ_X	$\rho_{x,x}$								
			$\beta_\varepsilon(0.44)$	$\beta_\varepsilon(1.06)$	$\beta_\varepsilon(3.9)$	$\Delta\beta_{ac}$	$\Delta\beta_{id}$	$\Delta\beta_c$	t	a	q
$\beta_\varepsilon(0.44)$, km^{-1}	0.2423	0.129	1.00	0.831	0.565	0.930	0.800	0.711	0.297	0.532	0.325
$\beta_\varepsilon(0.48)$, km^{-1}	0.2184	0.121	0.993	0.836	0.581	0.916	0.837	0.719	0.306	0.527	0.298
$\beta_\varepsilon(0.52)$, km^{-1}	0.1990	0.112	0.980	0.845	0.586	0.893	0.865	0.723	0.308	0.510	0.271
$\beta_\varepsilon(0.55)$, km^{-1}	0.1760	0.101	0.960	0.861	0.601	0.853	0.886	0.736	0.319	0.494	0.235
$\beta_\varepsilon(0.69)$, km^{-1}	0.1414	0.0797	0.909	0.882	0.644	0.752	0.900	0.769	0.366	0.462	0.143
$\beta_\varepsilon(0.87)$, km^{-1}	0.1300	0.0706	0.840	0.902	0.738	0.615	0.834	0.843	0.430	0.459	0.058
$\beta_\varepsilon(1.06)$, km^{-1}	0.1059	0.0541	0.831	1.00	0.719	0.587	0.732	0.879	0.380	0.390	0.072
$\beta_\varepsilon(1.6)$, km^{-1}	0.0950	0.0456	0.803	0.938	0.821	0.571	0.562	0.959	0.415	0.439	0.079
$\beta_\varepsilon(2.17)$, km^{-1}	0.0754	0.0368	0.652	0.855	0.904	0.392	0.416	0.980	0.432	0.351	−0.063
$\beta_\varepsilon(3.9)$, km^{-1}	0.0688	0.0375	0.565	0.719	1.00	0.336	0.287	0.940	0.461	0.408	−0.053
$\Delta\beta_{ac}$, km^{-1}	0.0831	0.0591	0.930	0.587	0.336	1.00	0.692	0.461	0.149	0.503	0.449
$\Delta\beta_{id}$, km^{-1}	0.0461	0.0395	0.800	0.732	0.287	0.692	1.00	0.449	0.236	0.355	0.169
$\Delta\beta_c$, km^{-1}	0.0797	0.0384	0.711	0.879	0.940	0.461	0.449	1.00	0.453	0.419	−0.006
t, °C	14.55	7.55	0.297	0.380	0.461	0.149	0.236	0.453	1.00	0.634	−0.319
a, g/m^3	8.060	3.37	0.532	0.390	0.408	0.503	0.355	0.419	0.634	1.00	0.476
q, %	62.67	21.0	0.325	0.0720	−0.053	0.449	0.169	−0.006	−0.319	0.476	1.00

Table 2

Parameter	$\overline{X}$	σ_X	$\Delta\beta_{ac}$	$\Delta\beta_{id}$	$\Delta\beta_c$	t	a	q
1	2	3	4	5	6	7	8	9
May, N = 243								
$\Delta\beta_{ac}$, km^{-1}	0.0446	0.0257	1.00	0.480	0.197	0.148	0.506	0.274
$\Delta\beta_{id}$, km^{-1}	0.0260	0.0153	0.480	1.00	0.429	0.151	0.166	0.043
$\Delta\beta_c$, km^{-1}	0.0745	0.0248	0.197	0.429	1.00	0.425	0.036	−0.289
t, °C	14.23	6.227	0.148	0.151	0.425	1.00	0.132	−0.741
a, g/m^3	6.325	1.732	0.506	0.166	0.036	0.132	1.00	0.515
q, %	54.76	21.86	0.274	0.043	−0.289	−0.741	0.515	1.00
June, N = 197								
$\Delta\beta_{ac}$, km^{-1}	0.1016	0.0507	1.00	0.814	0.670	−0.177	0.370	0.394
$\Delta\beta_{id}$, km^{-1}	0.0779	0.0360	0.814	1.00	0.897	0.012	0.190	0.147
$\Delta\beta_c$, km^{-1}	0.0833	0.0349	0.670	0.897	1.00	0.125	0.129	0.039
t, °C	19.85	3.987	−0.177	0.012	0.125	1.00	−0.225	−0.799
a, g/m^3	10.84	2.424	0.370	0.190	0.129	−0.225	1.00	0.745
q, %	65.67	21.74	0.394	0.147	0.039	−0.799	0.745	1.00
July, N = 224								
$\Delta\beta_{ac}$, km^{-1}	0.0885	0.0464	1.00	0.762	0.432	−0.231	0.399	0.465
$\Delta\beta_{id}$, km^{-1}	0.0262	0.0170	0.762	1.00	0.544	0.026	0.324	0.202
$\Delta\beta_c$, km^{-1}	0.1046	0.0414	0.432	0.544	1.00	0.407	0.210	−0.170
t, °C	19.84	5.278	−0.231	0.026	0.407	1.00	0.038	−0.808
a, g/m^3	10.69	2.399	0.399	0.324	0.210	0.038	1.00	0.538
q, %	65.33	22.84	0.465	0.202	−0.170	−0.808	0.538	1.00
August, N = 239								
$\Delta\beta_{ac}$, km^{-1}	0.1004	0.0678	1.00	0.849	0.539	0.040	0.612	0.378
$\Delta\beta_{id}$, km^{-1}	0.0462	0.0343	0.849	1.00	0.629	0.219	0.587	0.175
$\Delta\beta_c$, km^{-1}	0.0838	0.0453	0.539	0.629	1.00	0.388	0.500	−0.085
t, °C	17.25	5.210	0.040	0.219	0.388	1.00	0.414	−0.728
a, g/m^3	9.954	2.352	0.612	0.587	0.500	0.414	1.00	0.279
q, %	69.00	19.84	0.378	0.175	−0.085	−0.728	0.279	1.00

Table 2. Continued

1	2	3	4	5	6	7	8	9
September, N = 294								
$\Delta\beta_{ac}$, km^{-1}	0.0918	0.0751	1.00	0.672	0.477	0.362	0.754	0.532
$\Delta\beta_{id}$, km^{-1}	0.0643	0.0548	0.672	1.00	0.583	0.633	0.678	0.162
$\Delta\beta_c$, km^{-1}	0.0757	0.0353	0.477	0.583	1.00	0.409	0.325	0.011
t, °C	11.08	5.616	0.362	0.633	0.409	1.00	0.639	–0.237
a, g/m^3	6.523	2.473	0.754	0.678	0.325	0.639	1.00	0.568
q, %	63.13	18.28	0.532	0.162	0.011	–0.237	0.568	1.00
October, N = 154								
$\Delta\beta_{ac}$, km^{-1}	0.0699	0.0413	1.00	0.614	0.329	0.029	0.366	0.422
$\Delta\beta_{id}$, km^{-1}	0.0306	0.0165	0.614	1.00	0.406	0.272	0.203	0.050
$\Delta\beta_c$, km^{-1}	0.0479	0.0202	0.329	0.406	1.00	–0.283	–0.125	0.125
t, °C	2.903	5.299	0.029	0.272	–0.283	1.00	0.543	–0.319
a, g/m^3	3.396	1.316	0.366	0.203	–0.125	0.543	1.00	0.584
q, %	56.68	17.48	0.422	0.050	0.125	–0.319	0.584	1.00

The values of the parameters $\Delta\beta_{ac}$, $\Delta\beta_{id}$, and $\Delta\beta_c$ were determined as the differences between linear combinations (averaged over the wavelength range) of the coefficients $\beta_\varepsilon(\lambda)$:

$$\Delta\beta_{ac} = [\beta_\varepsilon(0.44) + \beta_\varepsilon(0.48) + \beta_\varepsilon(0.55)]/3 - [\beta_\varepsilon(0.69) + \beta_\varepsilon(0.87) + \beta_\varepsilon(1.06)]/3, \quad (1)$$

$$\Delta\beta_{id} = [\beta_\varepsilon(0.69) + \beta_\varepsilon(0.87) + \beta_\varepsilon(1.06)]/3 - [\beta_\varepsilon(1.6) + \beta_\varepsilon(2.17) + \beta_\varepsilon(3.9)]/3, \quad (2)$$

$$\Delta\beta_c = [\beta_\varepsilon(1.6) + \beta_\varepsilon(2.17) + \beta_\varepsilon(3.9)]/3. \quad (3)$$

Let us note that this technique for isolation of the components is conditional, but, as the results of subsequent analysis show, the values of the components $\Delta\beta_{ac}$, $\Delta\beta_{id}$, and $\Delta\beta_c$ give quite an adequate idea of the relative contributions of the particles of different size ranges to the total aerosol extinction, including the idea of their mutual variability under the effect of different atmospheric factors.

Among the data shown in Table 1 one should note a significant correlation between variations of the aerosol extinction in the visible and IR ranges ($\rho > 0.5$), as well as between the parameters $\Delta\beta_{ac}$ and $\Delta\beta_c$ ($\rho = 0.46$). It is an evidence of the atmospheric processes, which lead to a correlated change in the size spectrum of particles of the near-ground haze in the entire size range. The correlation between variations of $\beta_\varepsilon(\lambda)$ and meteorological parameters of the atmosphere is also well seen. In particular, the aerosol extinction of the short-wave radiation has positive correlation with the relative humidity of air ($\rho_{\Delta\beta_{ac},\, q} = 0.45$), while that in the IR range well correlates with the air temperature ($\rho_{\Delta\beta_c,\, t} = 0.45$). Besides, significant correlation of the parameters $\Delta\beta_{ac}$ and $\Delta\beta_{id}$, and absolute humidity of the air is observed ($\rho_{\Delta\beta_{ac},\, a} = 0.50$, $\rho_{\Delta\beta_{id},\, a} = 0.36$). This correlation for the accumulative component is higher than that with the relative humidity and temperature. Analogous correlations between the components $\Delta\beta_{ac}$, $\Delta\beta_{id}$, $\Delta\beta_c$, and meteorological parameters in different measurement periods are also seen in the data presented in Table 2.

To reveal the causes of the aforementioned facts, let us consider transformation of the statistical characteristics of the spectral aerosol extinction coefficients at different scales of data averaging.

Seasonal variability of the spectral aerosol extinction coefficients

Figure 1 shows the monthly mean spectra of the coefficients $\beta_\varepsilon(\lambda)$ since May and until October (Figs. 1*a* and *b*), their rms deviations $\sigma_\beta(\lambda)$ (Fig. 1*c*), and three first eigenvectors $\varphi_i(\lambda)$ of the autocorrelation matrix $\rho_{\beta,\beta}$ (Figs. 1*d–f*). This set of parameters was used as the basis for comparing the experimental data and theory.

Comparison was performed using not individual realizations, but the properties of corresponding statistical ensembles of $\beta_\varepsilon(\lambda)$, which were represented in the form of expansion in the orthonormalized system of eigenvectors of the autocorrelation matrix[10] $\rho_{\beta\beta}$:

$$\beta_\varepsilon^{(i)}(\lambda_j) = \overline{\beta_\varepsilon(\lambda_j)} + \sum_{k=1}^{m} C_k^{(i)} \varphi_k(\lambda_j), \quad (4)$$

where $C_k^{(i)}$ are the expansion coefficients calculated by the formula

$$C_k^{(i)} = \sum_{k=1}^{m} [\beta_\varepsilon^{(i)}(\lambda_j) - \overline{\beta_\varepsilon(\lambda_j)}]\, \varphi_k(\lambda_j). \quad (5)$$

The variance of the coefficients $C_k^{(i)}$ is determined by the eigenvalues of the correlation matrix μ_k according to the following formula:

$$\mu_k = \frac{1}{n} \sum_{i=1}^{n} \left| C_k^{(i)} \right|^2. \quad (6)$$

The eigenvectors $\varphi_k(\lambda_j)$ and eigenvalues μ_k of the autocorrelation matrix were calculated by the Jacobi method.[10]

It is seen from the data shown in Fig. 1 that the least values of the aerosol extinction coefficients in the entire wavelength range were observed in May and October. The minimum of the variability of the parameter $\beta_\varepsilon(\lambda)$ also was observed in these months. Maximum of the turbidity in the visible range was observed in June, and that in the IR range in July.

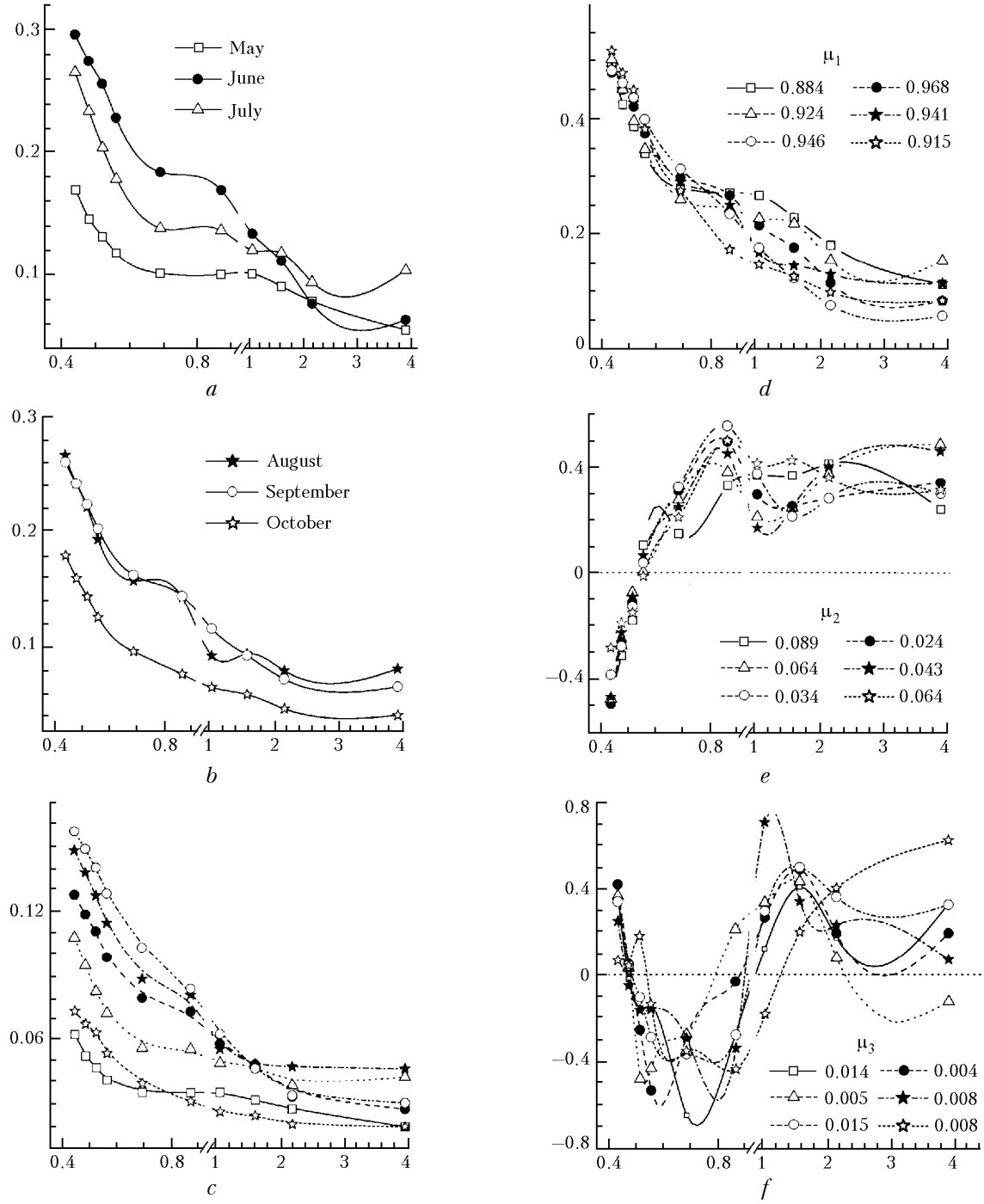

Fig. 1. Statistical characteristics of the aerosol extinction in six subarrays obtained in different months.

It is worthy to note here that, according to the experience of long-term investigations, maximum values of the aerosol extinction coefficient in the IR range and its greatest variability are continuously observed in July. Most likely, this is caused by the well-developed convection in this season and by the intense emission of coarse aerosol from the underlying surface. Maximum variability of $\beta_\varepsilon(\lambda)$ in the short-wave range is observed in August and September, that is caused by periodic intrusion of weakly smoked air masses formed in the west regions of Russia resulting from strong peatbog fires to the region of observations.

Analysis of the eigenvectors $\varphi_i(\lambda)$ and eigenvalues μ_k of the autocorrelation matrix shows that the maximum variance of the aerosol extinction coefficients $\beta_\varepsilon(\lambda)$ corresponds to the first vector $\varphi_1(\lambda)$, which characterizes the portion of sign-correlated variations of the parameter $\beta_\varepsilon(\lambda)$ in the entire wavelength range. In particular, the portion of the variance corresponding to the first eigenvector since June until September was from 92 to 97%, and in May and

October it decreased to 88 and 91%, respectively (see Fig. 1*d*). The portion of the variance corresponding to the second (with alternating signs) vector $\varphi_2(\lambda)$ is from 2.4% in June to 8.9% in May. Let us note that this vector has one sing-change point, which lies in the range of the wavelength of $\lambda = 0.55$ μm for all the arrays presented. A sufficiently large portion of the variance corresponding to this vector means that there are physical processes in the atmosphere, making the coefficients $\beta_\varepsilon(\lambda)$ in visible range to increase, while to decrease in the IR range, and *vise versa*. For example, one can consider diurnal behavior of the air relative humidity and temperature on a summer day as such a process. As underlying surface gets heated in the morning, convective emission of coarse aerosol into the near-ground layer of the atmosphere intensifies, that leads to an increase in the aerosol extinction in the entire wavelength range, including the IR range. However, relative humidity of the air decreases simultaneously with the increase of temperature that leads to a decrease of the aerosol extinction coefficients in the visible wavelength range.

Essentially smaller portion of the variance of $\beta_\varepsilon(\lambda)$ corresponds to the third vector, from 0.4 to 1.5%. It is extremely difficult to interpret the spectral behavior of this vector with alternating sign, however, one can say about general peculiarities of the spectral dependences of $\varphi_3(\lambda)$ in all subarrays.

Diurnal variability of the spectral aerosol extinction coefficients

It is seen from the data presented in Tables 1 and 2 that the variations of the coefficient $\beta_\varepsilon(\lambda)$ and its components $\Delta\beta_{ac}$, $\Delta\beta_{id}$, and $\Delta\beta_c$ are related to the variations of the meteorological parameters of the atmosphere both in the general array and in individual seasons as well. This allows one to say more certainly that there exist some physical processes affecting the optical properties of the atmosphere, based on the diurnal behavior of the meteorological parameters. Taking into account that the strongest correlation between the aerosol extinction and relative humidity of the air is observed in the short-wave range (see Table 1), let us consider the diurnal dynamics of the parameters $\Delta\beta_{ac}$ and q since May and until October (Fig. 2).

The curves in this figure show that the diurnal behavior of the aerosol extinction component due fine aerosol fraction since May until October, on the average, follow the behavior of the relative humidity of the air. However, this peculiarity has not been observed in October. Most likely, this was caused by low humidity in this month. The mean value of the relative humidity in the morning maximum in October was only ~ 65% that is essentially lower than the level of water vapor condensation on aerosol particles.

On the whole, the diurnal behavior of the extinction component $\Delta\beta_c$ (Figs. 3*a* and *b*) due to coarse aerosol fraction well agrees with the diurnal variation of the air temperature t (Figs. 3*c* and *d*) only in June, July, and August, when the highest temperatures have been observed, and, hence, the convective flows have been developed very well. As the air temperature decreases in May and September, correlation between $\Delta\beta_c$ and t significantly weakens, and diurnal behavior of $\Delta\beta_c$ in October has nothing to do with the diurnal behavior of temperature.

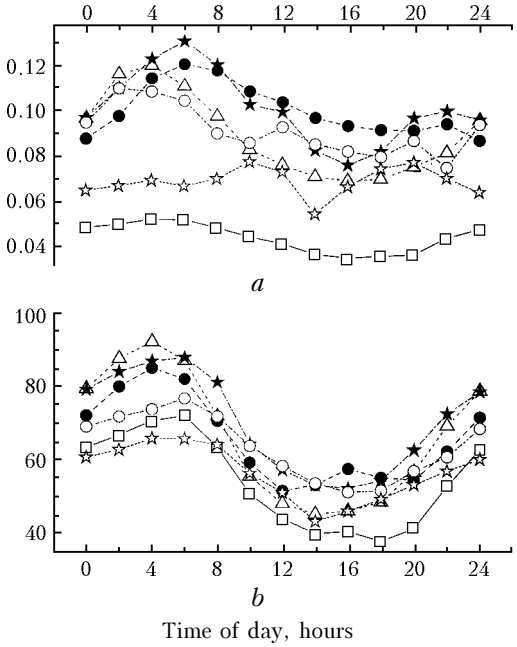

Fig. 2. Diurnal behavior of the aerosol extinction of submicron particles (*a*) and of the air relative humidity from spring to fall (*b*): –□– May, ● June, Δ July, ∗ August, ○ September, ☆ October.

The diurnal behavior of the extinction component $\Delta\beta_{id}$ due to intermediate aerosol fraction observed since May until October (without reference to meteorological parameters) is shown in Fig. 4. It is seen from this figure that no general regularities of the diurnal behavior of the extinction of radiation by intermediate aerosol fraction are observed in all measurement periods. The largest $\Delta\beta_{id}$ values were observed in June (up to 0.09 km^{-1}) and in September (up to 0.07 km^{-1}). Let us note that, according to some signs, the air masses containing smoke aerosol of remote transfer[15,16] prevailed in the region of measurements during these periods. The values of the extinction component due to intermediate aerosol fraction in August were 0.04 to 0.05 km^{-1}, and its diurnal behavior, on the average, corresponded to that observed in September. The least values of this component were observed in July and May (0.02 to 0.03 km^{-1}).

When studying the role of the intermediate-size aerosol fraction in the atmospheric optics, the problem of origin of this aerosol is of a significant interest. Thus, some preliminary estimates can be obtained in studying the diurnal variability of the mean components $\Delta\beta_{ac}$, $\Delta\beta_{id}$, and $\Delta\beta_c$. The diurnal behavior of these components in July 2002 is shown in Fig. 5 as an example. It is seen that in this specific case the

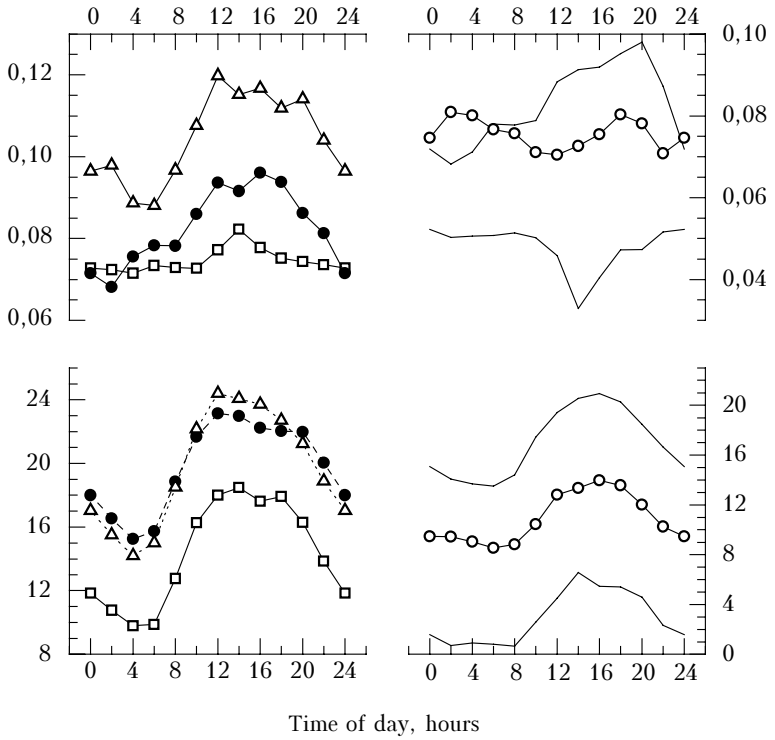

Fig. 3. Transformation of the diurnal behavior of the aerosol extinction of coarse particles and air temperature from spring to fall (see notations in Fig. 2).

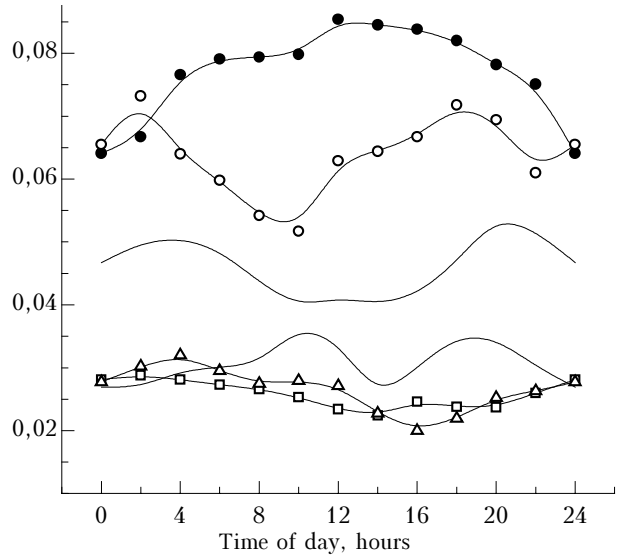

Fig. 4. Seasonal transformation of the diurnal behavior of the extinction by intermediate-size aerosol fraction (see notations in Fig. 2).

dynamics of the extinction component due to intermediate-size aerosol fraction significantly better agrees with the diurnal behavior of the extinction component caused by the accumulative aerosol fraction rather than with the component due to extinction by the coarse aerosol fraction. This allows us to conclude that, most likely, in July the intermediate fraction of aerosol was formed from the accumulative fraction. Of course, later on this supposition is to be checked up by observations in other periods.

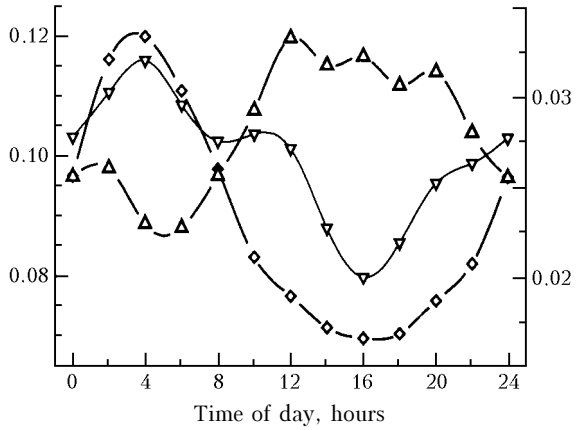

Fig. 5. Diurnal behavior of the components of aerosol extinction $\Delta\beta_{ac}$, $\Delta\beta_{id}$, and $\Delta\beta_c$ in July 2002.

In order to have better grounds for speculations on the physical processes leading to one or another changes in the spectra of the aerosol extinction coefficients of the near-ground haze, the data are needed on the corresponding variations of the atmospheric aerosol microstructure.

Microstructure interpretation of the optical data using individual realizations of $\beta_\varepsilon(\lambda)$ can be done, in particular, by the methods for solving the inverse problem.[11] However, the unavoidable errors in measuring the aerosol extinction coefficients $\beta_\varepsilon(\lambda)$ as well as *a priori* ambiguity and spectral variations of the refractive index of different aerosol fractions at different wavelengths often lead to an ambiguous estimate of the disperse composition of the near-ground

haze. Therefore, in addition to the data on microstructure obtained on the basis of solving the inverse problem of the aerosol light-scattering, it is also interesting to consider the results of direct "microphysical modeling" of the variability of the aerosol extinction in the atmosphere.

Technique of modeling

As was mentioned above, the elements of the technique developed for modeling were presented in part in Ref. 7. The idea of the approach is in the numerical modeling of an ensemble of realizations of the aerosol extinction coefficients $\beta_\varepsilon(\lambda)$ based on the algorithms of the Mie theory using the microphysical data, statistical variability of which provides for the spectral dependence of the elements of the orthogonal expansion (4) close to that measured under different meteorological conditions.

As known, the coefficients $\beta_\varepsilon(\lambda)$ obtained using the long-path absorption method of the atmospheric transmission are averaged over significantly larger scattering volume as was done in Ref. 7. Therefore, in numerical modeling the ensemble of realizations of the spectral vectors $\beta_\varepsilon(\lambda)$, a slightly modified technique from Ref. 7 was used for determining the disperse composition and the refractive index of the particulate mater of the haze.

The superposition of six lognormal modes was used at the first stage for setting the characteristic variations of the shape of the number density size-distribution function $f(r)$. Three of them were intended for description of the possible structure variations of the particle size spectrum in the size range of the accumulative fraction (r = 0.05–0.45 μm) and the same number was used in the intermediate size range and for the coarse aerosol fraction (r = 0.45–9.0 μm):

$$f(r) = \frac{\mathrm{d}N_\mathrm{c}}{\mathrm{d}r} = A\, r^{-3} \sum_{i=1}^{K} M_i \exp\left\{-b_i \left[\ln\left(r / r_i\right)\right]^2\right\}, \ \mu\mathrm{m}^{-1}\,\mathrm{cm}^{-3}, \quad (7)$$

where r_i, b_i, A, M_i are the model parameters, N_c is the number density, cm^{-3}. In order for the model spectrum to be not beyond the disperse composition characteristic of the atmospheric haze, the ensemble of realization of $f(r)$ was formed by the method of random selection of the parameters of the model (7) from the ranges of variations shown in Table 3. The mean, minimum, and maximum values of the statistical variations of the parameters r_i, b_i and $F_i = AM_i$ are presented here according to the qualitative determination of the fraction elements.

At the second stage, in order to take into account smaller random structure variations of the size spectrum of the atmospheric haze, each of the modes was divided into 3 to 6 subfractions. The technique applied for dividing the spectrum at transition from the first stage to the second one provided for the invariance of the characteristic peculiarities of the disperse composition of the atmospheric haze. The norm of the deviation of the spectral dependences of the aerosol extinction coefficient calculated at two stages did not exceed 5–10%.

Table 3. The values of the parameters of the particle size-distribution function (7)

Parameters of the distribution mode	Interval value			Distribution (type)
	minimum	mean	maximum	
Fraction 1 (microdisperse)				
r_1, μm	0.07	0.11	0.14	uniform
b_1	3.0	5.0	9.0	uniform
$\ln F_1$	3.0	4.5	6.0	normal
Fraction 2 (accumulative 1)				
r_2, μm	0.17	0.23	0.30	uniform
b_2	6.0	8.0	12	uniform
$\ln F_2$	1.0	2.75	4.5	normal
Fraction 3 (accumulative 2)				
r_2, μm	0.2	0.3	0.40	uniform
b_2	6.0	8.0	12	uniform
$\ln F_3$	0.7	2.4	4.0	normal
Fraction 4 (intermediate 1)				
r_2, μm	0.55	0.69	1.1	uniform
b_2	6.0	8.0	16.0	uniform
$\ln F_4$	0.28	2.0	4.0	normal
Fraction 5 (intermediate 2)				
r_3, μm	1.26	1.49	1.98	uniform
b_3	4.0	8.0	16.0	uniform
$\ln F_5$	0.6	2.1	3.7	normal
Fraction 6 (coarse)				
r_4, μm	2.8	3.4	4	uniform
b_4	4	8.0	12	uniform
$\ln F_6$	0.4	2.1	3.8	normal

The sample of the values of 18 parameters of the model (7) and the characteristic peculiarities of an individual realization of the disperse composition of the near-ground haze were determined at the first stage using random-number generator technique. Then at the second stage the specific realization $f(r)$ underwent additional more fine random deformations inside each of the six modes of the distribution (7). Illustration of the technique for dividing the principal modes of the distribution into additional subfractions is schematically shown in Fig. 6*a*, and a sample (32 realizations) of statistically modeled spectra and the model size spectrum averaged over 512 realization (May 2002) are shown in Fig. 6*b* as an example. Solution of the system of linear equations written as a condition of invariance of the total cross sections, volume and number density of particles was used for estimating the parameters of the modes of the final expansion $f(r)$.

Thus, the statistical ensemble of random realizations of the haze particle size spectrum was formed, which has quite fine structure on the size scale and reflects the fraction composition characteristic of the atmospheric haze.

Besides, deformations of the spectrum $f_i(r)$ related to the dynamics of relative humidity of the air q were taken into account in the algorithm of numerical modeling of an individual realization $f_i(r)$. The values q were chosen using random-number generator technique with the normal distribution about the mean value q_c in the interval from 0.2 to 0.95.

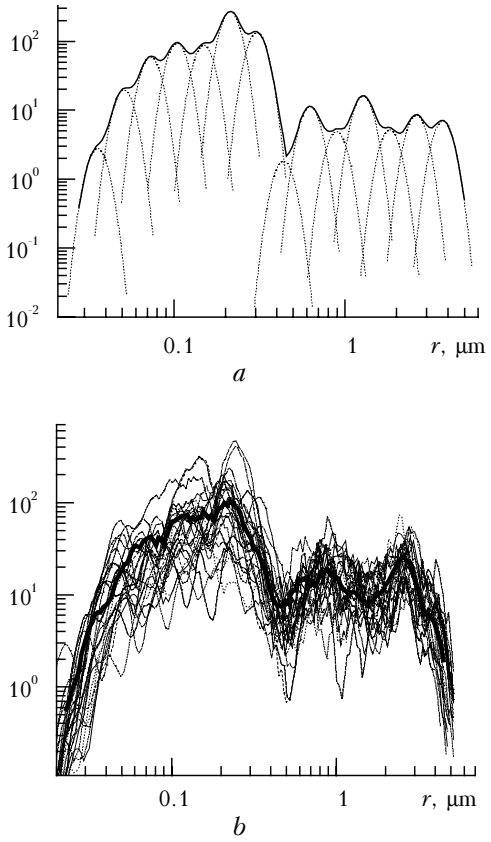

Fig. 6. Diagram of splitting of individual modes of a random distribution at the second stage of modeling (*a*), a sample of individual realizations of the size spectrum of the near-ground haze (*b*).

Since the measurements of the aerosol extinction in the haze were carried out in the wavelength range $\lambda = 0.4–3.9$ μm, the data from Ref. 6 were used for numerical modeling, which contained the optical constants of different chemical elements and compounds comprising the substance of the aerosol particles in a wide wavelength range. On the whole, 17 elements and compounds was taken into account in calculations.

The numerical experiments carried out earlier[3,12] showed that not all peculiarities of the spectral variations of the real and imaginary parts of the refractive index $m_i(\lambda)$ play the priority role in the formation of the spectral behavior of the aerosol light-scattering parameters, but only some most important absorption bands. Therefore, in modeling the variability of the dielectric properties of the particulate matter of different fractions, the qualitatively certain sample $m_i(\lambda)$ was used, containing approximately 5 to 8 spectral peculiarities. In particular, the technique for forecasting local spectral variability of the real and imaginary parts of $m_i(\lambda)$ described by the model of self-quenching oscillator[13] was used for synthesis of the styled spectral peculiarities $m_i(\lambda)$. The spectral dependences $m(\lambda)$ of minerals were mainly used in modeling the optical properties of the coarse fraction for determination of the absorption bands, while the data on the fine fraction were formed on the basis of complicated chemical complexes, in particular, the mixture of ammonium sulfate, sulfur acid, and water. Variations of the soot component were taken into account according to known principle of external mixture, when the spectral values of the complex refractive index were corrected for the volume proportions of the components. The weight proportions between the components were set using random-number generator technique with the normal distribution about the mean value.

As was shown (see Figs. 2 and 3), quite stable variations of the mean content of different aerosol fractions are observed in the near-ground layer, which also were taken into account when forming the statistical ensemble of the haze states.

The experimental data shown in Figs. 1*a–c* contain quite detailed information on the spectral variability of $\beta_\varepsilon(\lambda)$ in the time interval covering approximately three seasons. The model estimates were constructed so that one can reveal the peculiarities of variations of the optical and microphysical properties of the near-ground haze during several months. To do this, we have set the specific statistics of variation of the parameters of the model (7) and the spectral dependence of the refractive index, and obtained more than 500 realizations of $\beta_\varepsilon(\lambda)$ for each month.

At the first stage, the initial values of the parameters of model (7) for each month were determined by the following algorithm. First, the modal radii of the fractions (on the logarithmic r scale) were assumed to be distributed uniformly: $r_i = 0.08$; 0.16; 0.32; 0.64; 1.28; and 2.56 μm. The values of the parameters b_i varied within one month and from month to month within the range from 3.0 to 9.0, but, on the whole, as subsequent calculations showed, the widths of the modes of the distributions of individual fractions differed from each other only insignificantly.

In order to carry out direct microphysical modeling of the statistical variability of the haze state, it is necessary to determine the microphysical parameters optimal for each month. The disperse composition characteristic of each month was determined using the monthly mean-weighted spectral dependence $\overline{\beta_\varepsilon(\lambda)}$ on the basis of the iterative technique.[11] The values of the parameters of model (7) necessary for direct modeling were estimated using the reconstructed, in this way, histograms of the particle size distribution $f(r_j)$. Then, when comparing the elements of orthogonal expansion (4) of the theoretical and experimental data, the initial values of model (7) were corrected. The statistics of variations of the microphysical parameters (7) was estimated depending on the specific peculiarities of the empirical material, and the characteristic values $r_{i\text{av}}$, $b_{i\text{av}}$, $F_{i\text{av}}$ for each of the aforementioned fractions were determined more accurately.

In forming the statistical ensemble of realizations of the near-ground haze particle size spectrum, the conclusions of Ref. 7 were used. As shown[7] the numerical estimates better approach to the empirical

data, if statistics of the variations of the parameters of model (7) r_i, b_i has a uniform distribution, and the value $\ln F_i$ obeys normal distribution. To set the normal distribution, quite a widespread way was used for transformation of a pair of independent values ξ_1 and ξ_2 uniformly distributed in the interval (0, 1) to the value

$$\eta_1 = \sqrt{-\ln \xi_1 \times \ln \sigma} \cos 2\pi\xi_2,$$

distributed normally. Here the value $\ln\sigma$ regulates the deviations of η_1 from the center of the interval of variations.

The specific values of the centers of variations of the parameters of model (7) for each month are presented in Table 4 (columns 2–4 and 8–10). The relative amplitudes of the variations of the parameters Δr, Δb, and $\Delta \ln F$ for each value are also shown here. In particular, for $\Delta r = (r_i^{\max} - r_i^{\min})/(2r_i)$, and the values of other parameters were determined in a similar way.

Results

The results of inversion of the 6-month mean spectral dependences $\overline{\beta_\varepsilon(\lambda)}$ are shown in Fig. 7*a*, and the particle size spectra are shown in Figs. 7*b–d* separately for May and June, July and August, September and October for better clarity. These data show that the peculiarities of the disperse composition of the near-ground haze at different stages of the experiment appear due to characteristics changes in the contents of particles in three size ranges. In particular, as absolute water vapor content and temperature increase from May to June (Fig. 3*c*), the significant shift of the size spectrum to the right is observed in the size range of the accumulative fraction (Fig. 7*b*). The increase of the amplitude of the diurnal oscillations of the relative humidity in June (Fig. 2*b*) favors this fact.

The significant, uncorrelated with neighbor intervals, variations of the intermediate fraction content and the change of the spectrum shape as a whole are observed in the size range from 0.45 to 2.0 μm. In particular, the enhanced content of the intermediate fraction in the size range from 0.4 to 0.9 μm, which directly adjoins the size range of the accumulative fraction, is observed in June and September in contrast to other months. At the same time, the observed change in the content of intermediate fraction in the size range from 0.9 to 1.8 μm weakly correlates with the change of the right-hand boundary of the accumulative fraction, the maximum of their optical effect is observed from May and until July.

Finally, according to the inversion performed, a sharp increase in the content of particles of the coarse fraction in the size range from 2.2 to 4.0 μm (see Fig. 7*c*) is observed in July, that corresponds to the increase of $\Delta\beta_c$ value (see Fig. 5) and is determined, as was mentioned above, by the increase of thermal instability of the boundary layer and intensification of the convective component of the turbulent mixing.

Comparison of the results obtained by numerical modeling of the mean spectral dependence $\overline{\beta_\varepsilon(\lambda)}$, the variance $\sigma_\beta(\lambda)$, and eigenvectors of correlation matrix (4) having similar characteristics calculated from the data of optical measurements in October 2002 is shown in Fig. 8.

Table 4. Values of the initial parameters of model (7)

Fraction No.	r_i	b_i	F_i	Δr	Δb	$\Delta \ln F$	r_i	b_i	F_i	Δr	Δb	$\Delta \ln F$
1	2	3	4	5	6	7	8	9	10	11	12	13
	May						*June*					
1	0.080	3.0	16.0	0.004	0.01	0.100	0.078	4.4	6.74	0.010	0.010	0.22
2	0.170	8.0	16.4	0.010	0.01	0.144	0.166	5.0	12.8	0.020	0.012	0.22
3	0.558	7.0	1.18	0.010	0.01	0.630	0.270	9.8	15.2	0.050	0.014	0.20
4	1.008	8.0	6.18	0.019	0.04	0.231	0.620	6.2	5.32	0.080	0.020	0.50
5	2.008	9.0	5.68	0.020	0.04	0.120	1.398	3.8	4.96	0.100	0.030	0.40
6	3.940	9.0	2.74	0.020	0.04	0.050	3.482	9.0	4.96	0.120	0.040	0.40
	July						*August*					
1	0.062	3.4	8.04	0.010	0.010	0.200	0.118	3.0	9.0	0.020	0.040	0.565
2	0.142	5.0	13.6	0.020	0.012	0.210	0.254	7.0	16.0	0.020	0.040	0.565
3	0.222	9.8	13.2	0.050	0.014	0.192	0.398	8.0	1.42	0.020	0.040	0.550
4	0.782	9.2	4.22	0.080	0.020	0.360	0.908	9.0	1.60	0.020	0.040	0.560
5	1.422	9.0	5.46	0.040	0.020	0.380	1.608	9.0	5.44	0.020	0.040	0.570
6	2.938	9.0	13.96	0.020	0.020	0.200	3.000	9.0	7.20	0.020	0.040	0.480
	September						*October*					
1	0.065	5.6	5.84	0.03	0.01	0.570	0.076	1.6	7.2	0.002	0.004	0.684
2	0.126	5.8	11.8	0.04	0.01	0.570	0.134	7.0	8.0	0.100	0.040	0.340
3	0.234	7.6	15.2	0.06	0.01	0.642	0.208	9.9	12.6	0.100	0.040	0.290
4	0.358	3.6	1.94	0.12	0.01	0.760	0.688	8.0	2.12	0.100	0.040	0.300
5	0.928	3.0	4.86	0.04	0.01	0.399	1.102	6.0	3.02	0.100	0.040	0.300
6	2.592	6.0	6.34	0.01	0.01	0.426	2.640	8.0	3.98	0.300	0.040	0.313

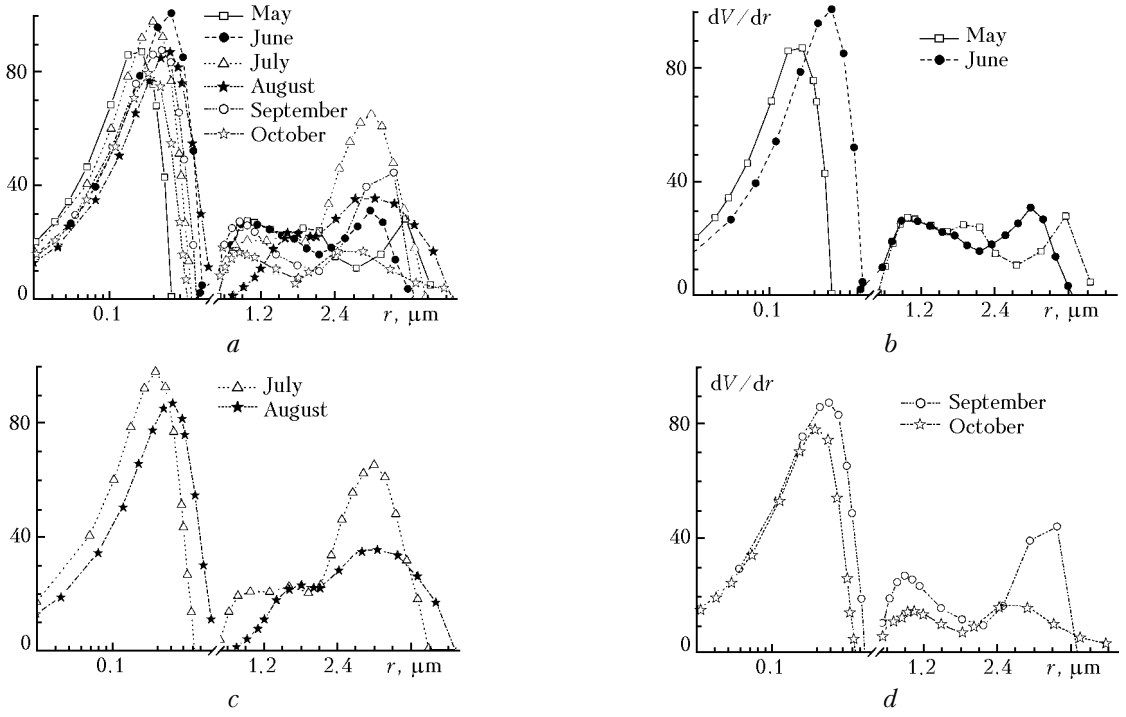

Fig. 7. The size spectra of the near-ground haze reconstructed by the method of inverting the monthly mean spectral dependences $\overline{\beta_\varepsilon(\lambda)}$.

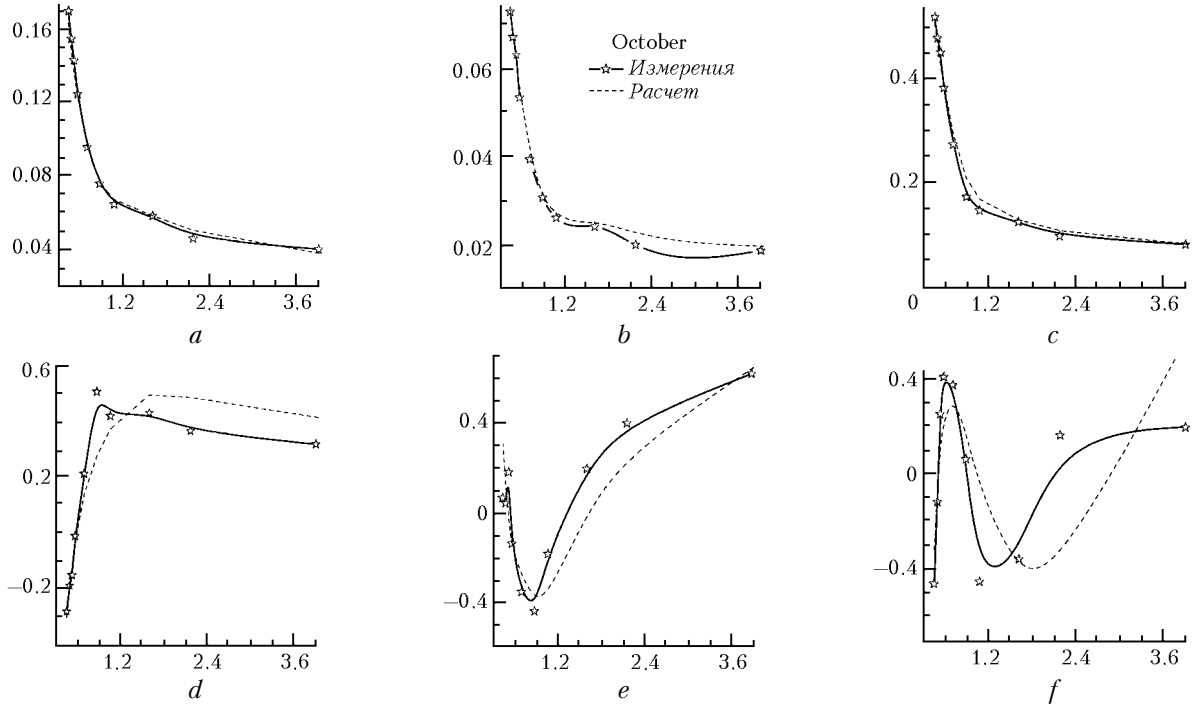

Fig. 8. Comparison of the results obtained by direct modeling of the parameters of orthogonal expansion (4) with the measured data.

As is seen, a satisfactory agreement of the model estimates with the measured data is achieved simultaneously for the mean spectral dependence (Fig. 8*a*), variance (Fig. 8*b*), and four eigenvectors (Figs. 8*c*–*f*). In spite of small differences in the spectral behavior of the calculated and measured data for the third $\varphi_3(\lambda)$ and fourth $\varphi_4(\lambda)$ vectors, the model estimates, on the whole, well represent the principal peculiarities. The agreement revealed is quite satisfactory, because, as has already been mentioned, the combined contribution of the components $\varphi_3(\lambda)$ and $\varphi_4(\lambda)$ to the total sum is approximately 1%.

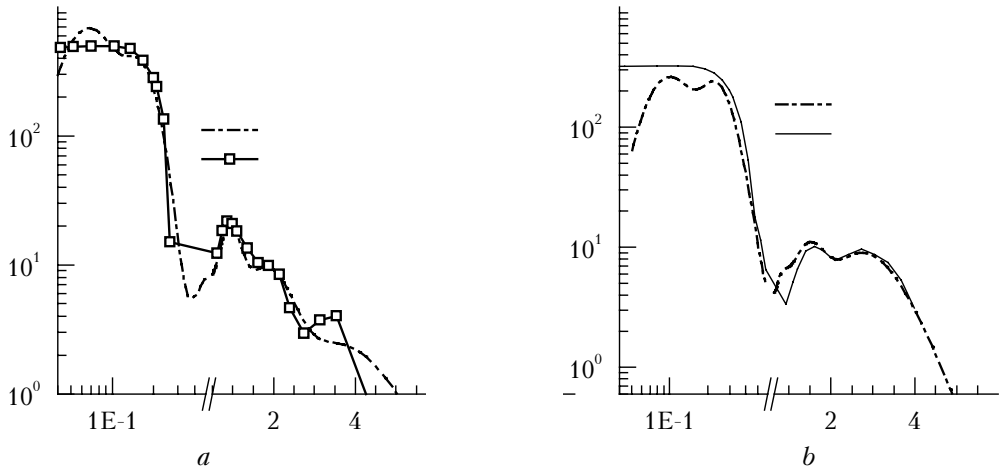

Fig. 9. The particle size spectra of the near-ground haze reconstructed by use of direct modeling (1) and by solving the inverse problem (2) for May and August.

Analogous results have also been obtained for other months. Thus, the closeness of the calculated and measured data on the set of optical characteristics analyzed is a good reason to suppose that the initial microphysical data used for calculations contain adequate information on the peculiarities of the atmospheric variability of the microstructure of the near-ground haze. Figure 9 presents comparison of particle-size distribution spectra reconstructed using direct modeling and from solution of the inverse problem for May and August. One should acknowledge that, in spite of a sufficient closeness of the spectra reconstructed from inversion of the mean spectral dependences $\overline{\beta_\varepsilon(\lambda)}$, to the mean weighted spectra obtained by use of statistical modeling, some differences are revealed being caused by technical peculiarities of the model estimates. The matter is that the best agreement between the calculated and empirical data is reached if the effect of relative humidity of the air has been taken into account at the second stage of modeling. The model corrections for the characteristic changes in the size spectrum $f_i(r)$ with relative humidity q were introduced in correlation with analogous corrections for the change of the real and imaginary parts of the refractive index of the particulate matter mainly only for the accumulative fraction.

The algorithm of correcting the spectrum was realized using the dynamics of the change of the integral values $Q_i(q)$ of separate subfractions (where $Q_i(q)$ means either number density $N_i(q)$ of particles, or their total cross section $S_i(q)$, or the volume $V_i(q)$). Based on the new values of the integral values of the size spectrum of a separate fraction (by the technique from Ref. 7) new values of the parameters $r_i(q)$, $b_i(q)$, $F_i(q)$ of model (7) were calculated. In addition, the statistics of variations of the parameter F_i at the first stage had normal distribution of the value $\ln(F_i)$. Therefore, in spite of the qualitative similarity of the spectra obtained using inversion technique and the most probable spectra $f_s(r)$, their mutual displacement along the ordinate axis and the abscissa axis is observed (Fig. 9). The shape of the spectrum $f_s(r)$ obtained using statistical comparison of the data in the size range of the accumulative fraction seems to be most adequate having in mind the properties of the actual near-ground hazes.

The problem of the characteristic variations of the optical effect of different fractions at transition from one spectral range to another is considered based on the set of individual realizations obtained. It is known that the optical effect of the particles of different size essentially depends not only on their cross section, but also on their relative content. As applied to the properties of the near-ground haze, this problem was discussed many times in a lot of papers.[1–7] The data obtained in October are shown in Fig. 10, which illustrate the correlation of the aerosol extinction coefficient $\beta_\varepsilon(\lambda)$ measured at $\lambda = 0.44$; 1.06; and 3.9 μm with the total cross section of the particles of the accumulative $\log(S_{123})$ and coarse $\log(S_{456})$ fractions. The value S_{123} is the total surface of three first subfractions S_1, S_2, and S_3; correspondingly, S_{456} is the sum of the three other subfractions S_4, S_5, S_6 of an individual realization. The values of the correlation coefficient for each pair in October are shown in Fig. 10, those for other months are presented in Table 5. The calculated data have been obtained using 512 individual realizations. The histograms of the frequency of occurrence N of the values of the aerosol extinction coefficient at three wavelengths are also shown in Figs. 10*a*, *d*, and *g*. The distribution of the logarithms of the total surface of aerosol particles of the accumulative S_{123} and coarse S_{456} fractions are presented by histograms in Figs. 10*j* and *k*.

As is seen from the data given in Table 5, the variability of the aerosol extinction in the near-ground layer at the wavelength of $\lambda = 0.44$ μm depends (practically on parity basis) on variations of the content of fine ($r < 0.45$ μm) and coarse ($r > 0.45$ μm) aerosols. The role of the accumulative fraction in forming $\beta_\varepsilon(\lambda)$ noticeably decreases if passing to the near IR range. The processes that govern the filling of the atmosphere with the coarse aerosol fraction have great significance here.

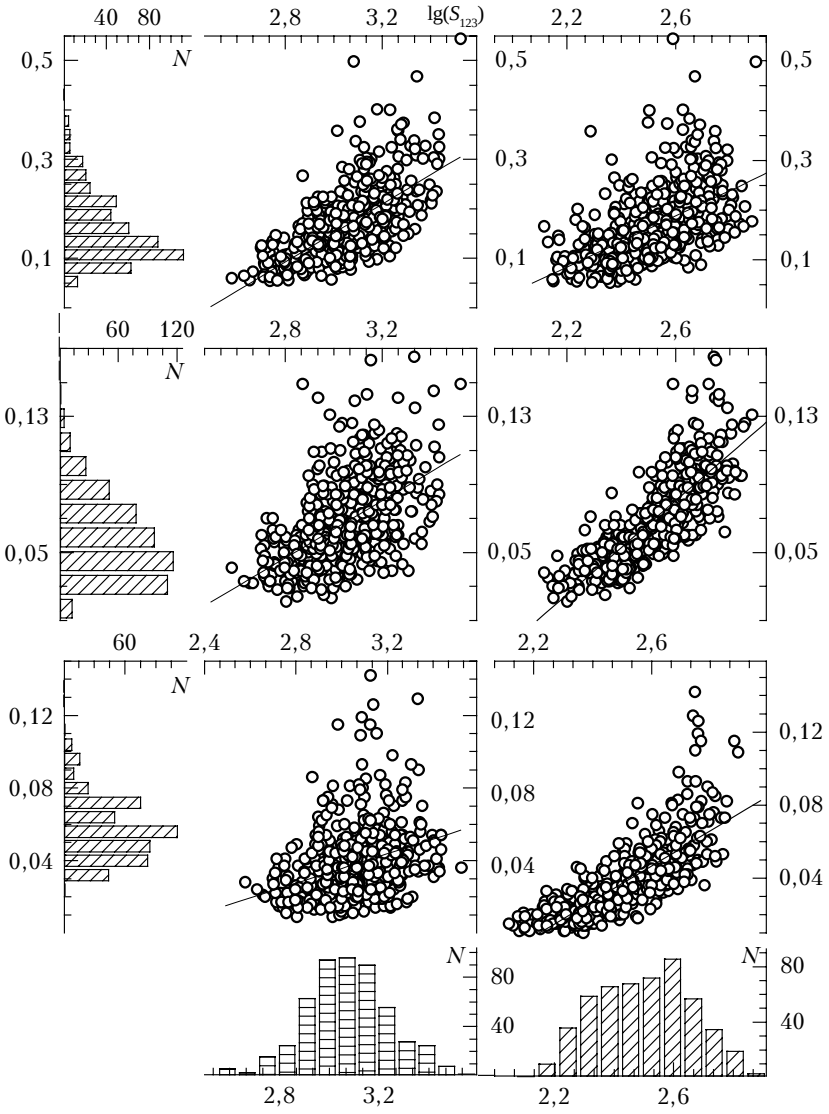

Fig. 10. Correlation of the values β_ε (λ = 0.44; 1.06; 3.9 μm) with the total surface area of the accumulative logS_{123} and coarse logS_{456} fractions.

Table 5. Coefficients of correlation between the measured parameter $\beta_\varepsilon^{(i)}(\lambda)$ and the total surface of the accumulative (ac) and coarse (c) aerosol fractions

Month	λ = 0.44 μm		λ = 1.06 μm		λ = 3.9 μm	
	$\rho_{\beta s}^{ac}$	$\rho_{\beta s}^{c}$	$\rho_{\beta s}^{ac}$	$\rho_{\beta s}^{c}$	$\rho_{\beta s}^{ac}$	$\rho_{\beta s}^{c}$
May	0.636	0.609	0.539	0.720	0.373	0.647
June	0.724	0.637	0.630	0.839	0.451	0.752
July	0.773	0.685	0.684	0.826	0.473	0.681
August	0.770	0.415	0.582	0.751	0.229	0.793
September	0.748	0.576	0.603	0.799	0.343	0.687
October	0.659	0.549	0.505	0.792	0.334	0.762

Analogous estimates obtained for narrower subfractions are shown in Table 6 and Fig. 11. As is seen in Table 6 and Fig. 11, the peculiarity of the formation of the disperse composition of hazes in different periods becomes quite clear if statistically analyzing the optical effect of different fractions. In particular, the second fraction plays the decisive role in the formation of aerosol extinction at the wavelength of 0.44 μm in the period from May and until August, while the particles of the intermediate size range play the main role at the wavelength of 1.06 μm.

Variations of the content of the particles of this size range in July are important for the formation of the aerosol extinction not only in the near IR range, but also in the short-wave range (0.44 μm). The peculiarities of the fractional formation of the aerosol extinction in September are caused, as was mentioned above, by the intrusion of cold air masses from Arctic (anomalous spectra $\beta_\varepsilon(\lambda)$), as well as by the disturbance of the near-ground haze resulting from the effect of forest fires. As is seen from Fig. 11, the relative contribution of fine particles to the formation of the aerosol extinction at the wavelength of λ = 3.9 μm in September essentially decreases, that agrees with other results.[14,15] It was noted in these papers that

the formation of $\beta_\varepsilon(\lambda)$ with the anomalous spectral behavior is caused by a sharp decrease in the content of the accumulative fraction and by the increasing role of the particles of the intermediate sizes.

Table 6. The values of the correlation coefficient $\rho^i_{\beta(\lambda)s}$ for different fractions

Fraction No.	May	June	July	August	September	October
			$\lambda = 0.44$ μm			
1	0.446	0.397	0.494	0.467	0.28	0.415
2	0.686	0.669	0.703	0.796	0.512	0.564
3	0.182	0.642	0.706	0.371	0.790	0.638
4	0.559	0.560	0.604	0.249	0.411	0.513
5	0.501	0.465	0.423	0.327	0.495	0.457
6	0.402	0.380	0.624	0.399	0.429	0.487
			$\lambda = 1.06$ μm			
1	0.39	0.402	0.517	0.345	0.307	0.287
2	0.441	0.544	0.566	0.568	0.389	0.498
3	0.272	0.587	0.638	0.388	0.571	0.463
4	0.699	0.742	0.732	0.364	0.429	0.684
5	0.552	0.593	0.502	0.722	0.722	0.646
6	0.382	0.467	0.736	0.523	0.523	0.702
			$\lambda = 3.9$ μm			
1	0.355	0.342	0.372	0.241	0.296	0.191
2	0.294	0.378	0.392	0.174	0.294	0.38
3	0.068	0.367	0.458	0.258	0.24	0.351
4	0.558	0.411	0.504	0.241	0.218	0.501
5	0.604	0.75	0.467	0.64	0.559	0.6
6	0.361	0.577	0.701	0.754	0.82	0.838

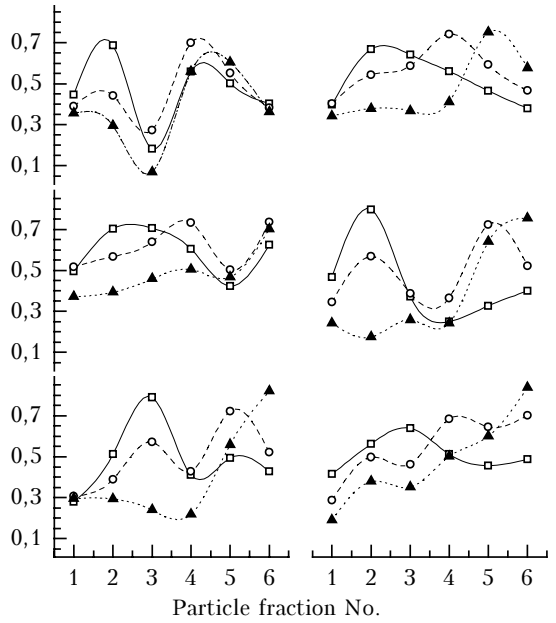

Fig. 11. Correlation between the measured values of the coefficients $\beta_\varepsilon(\lambda)$ and the contents of different fractions since May until October: —□— $\lambda = 0.44$, —○— $\lambda = 1.66$, —▽— $\lambda = 3.9$ μm.

As is easily seen from Figs. 10*a*, *d*, and *f*, maxima in the histograms of the $\beta_\varepsilon(\lambda)$ distribution are asymmetric being shifted to the range of small values. Besides, the scatter of points relative to the regression lines is indicative of the nonlinear dependence of $\beta_\varepsilon(\lambda)$ on the statistics of variations of even the values $\log(S_{123})$ and $\log(S_{456})$, and moreover, S_{123} and S_{456}.

So, the correlation of the values $\ln(\beta_\varepsilon(\lambda))$ with the value of the factor of filling the atmosphere by one or another fraction (Fig. 12) were considered using the results of statistical modeling. The logarithms of the values characterizing the specific volume content of particles, namely $\ln V_{123}$ and $\ln V_{456}$ were used instead of S_{123} and S_{456}.

The scatter of points about the regression line (Figs. 12*b*, *c*, *e*, *h*, and *i*) is smaller and more symmetric than that in Fig. 10. This fact allows us to use simple statistical mean functional dependence for the relation between the parameters $\beta_\varepsilon(\lambda)$ and V

$$\beta_\varepsilon(\lambda) = \beta_0(\lambda) V^\delta.$$

The values of the parameters $\beta_0 \cdot 10^{10}$ (km^{-1}) and δ as well as the correlation coefficients $\rho_{\ln\beta, \ln V}$ at three wavelengths are presented in Table 7. Correlation of the discussed parameters as applied to the size ranges of accumulative and coarse fractions is considered at each stage of measurements. Comparing the estimates presented in Tables 5 and 7, it is easy to see that, except for two or three episodes of measurements, the higher values of the correlation coefficient are characteristic of the relation of the logarithm of the extinction coefficient and the logarithm of the factor of specific aerosol filling of the atmosphere. The degree of nonlinear dependence of $\beta_\varepsilon(\lambda)$ on V_{123} for the accumulative fraction increases with the increase of the wavelength, while at $\lambda = 3.9$ μm this dependence on the factor of filling by the coarse aerosol fraction approaches the linear one, $\delta \sim 1.0$.

The size spectra of the near-ground haze obtained from the results of modeling the statistical variability of $\beta_\varepsilon^{(i)}(\lambda)$ dependences at different stages of the experiment are shown in Fig. 13. From these data one can isolate not only regular features of the seasonal variability of the disperse structure of the near-ground haze dS/dr, but also some specific peculiarities of the development of dS/dr under the effect of random factors, such as intrusion of smoke aerosol from the forest and peatbog fires. Naturally, the latter leads to some distortion of the seasonal dependences.

One can select the following factors among the stable ones affecting the change of the disperse composition of the near-ground haze:

– diurnal and seasonal variations of the air temperature and humidity;

– the value and the amplitude of the diurnal dynamics of the absolute and relative humidity of the air;

– intensification of the effect of convective component of turbulent diffusion in summer and, perhaps, the increase of the monthly mean duration of the sunshine.

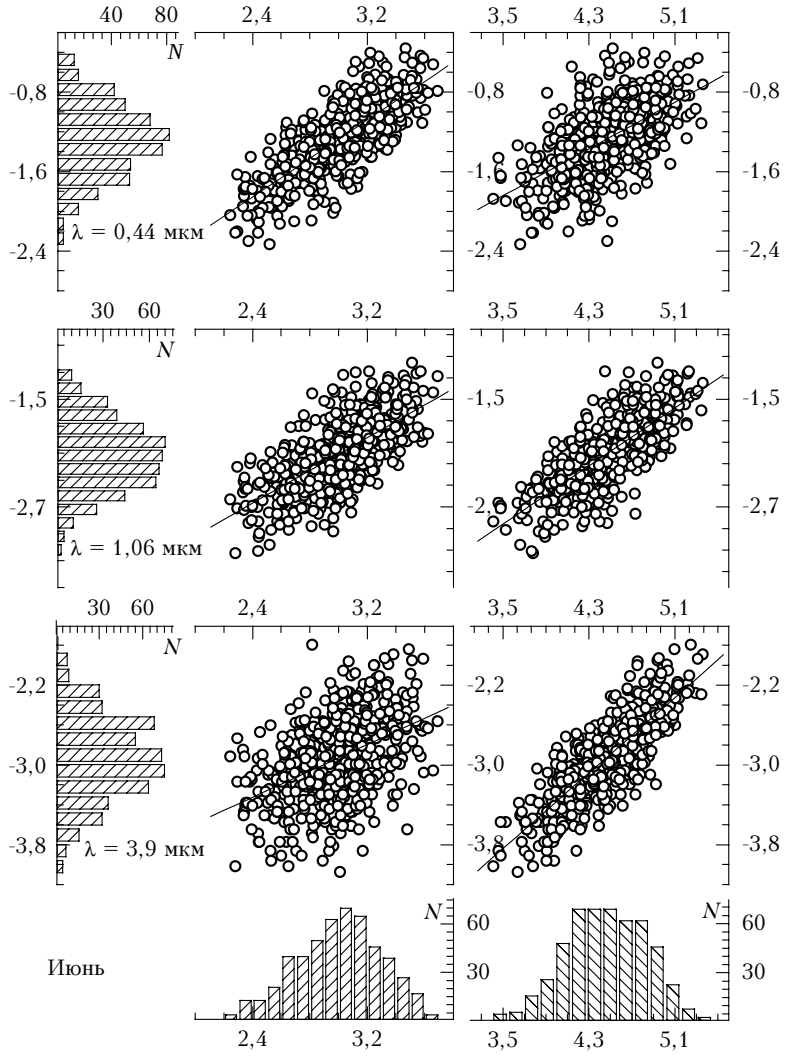

Fig. 12. Correlation of the values $\ln[\beta_\varepsilon(\lambda = 0.44;\ 1.06;\ 3.9\ \mu m)]$ with the logarithm of the specific volume of particles of accumulative $\ln V_{123}$ and coarse $\ln V_{456}$ fractions of aerosol.

Table 7

Month	λ = 0.44 μm			λ = 1.06 μm			λ = 3.9 μm		
	$\rho^{ac}_{\ln\beta\,\ln V}$	$\beta_0^{ac} \cdot 10^{10}$	δ	$\rho^{ac}_{\ln\beta\,\ln V}$	$\beta_0^{ac} \cdot 10^{10}$	δ	$\rho^{ac}_{\ln\beta\,\ln V}$	$\beta_0^{ac} \cdot 10^{10}$	δ
For accumulative fraction									
May	0.735	1.34383	0.85806	0.599	1.28236	0.67428	0.409	1.64983	0.42229
June	0.774	1.52339	0.96943	0.682	0.7846	0.91213	0.457	0.73732	0.66017
July	0.814	1.10691	1.06853	0.715	0.91245	0.87895	0.509	1.4146	0.66469
August	0.877	1.73641	0.85608	0.642	1.808	0.55703	0.265	2.62329	0.30482
September	0.872	2.43854	0.78918	0.661	2.42818	0.52236	0.361	2.38851	0.30936
October	0.773	1.61235	0.8676	0.639	1.12855	0.66478	0.471	0.65709	0.62855
For intermediate and coarse fractions									
	$\rho^{id,c}_{\ln\beta\,\ln V}$	$\beta_0^{id,c} \cdot 10^{10}$	δ	$\rho^{id,c}_{\ln\beta\,\ln V}$	$\beta_0^{id,c} \cdot 10^{10}$	δ	$\rho^{id,c}_{\ln\beta\,\ln V}$	$\beta_0^{id,c} \cdot 10^{10}$	δ
May	0.649	0.09138	1.17695	0.732	0.03391	1.27753	0.69	0.04508	1.10748
June	0.59	2.00477	0.59012	0.761	0.32262	0.81244	0.823	0.07783	0.94798
July	0.694	0.23471	0.92595	0.822	0.06928	1.02718	0.75	0.06883	0.99565
August	0.483	2.88354	0.4664	0.778	0.49233	0.66757	0.893	0.06974	1.01622
September	0.57	1.10018	0.69491	0.787	0.27074	0.83846	0.888	0.06368	1.02459
October	0.565	2.18989	0.50663	0.783	0.52697	0.65079	0.851	0.10546	0.90776

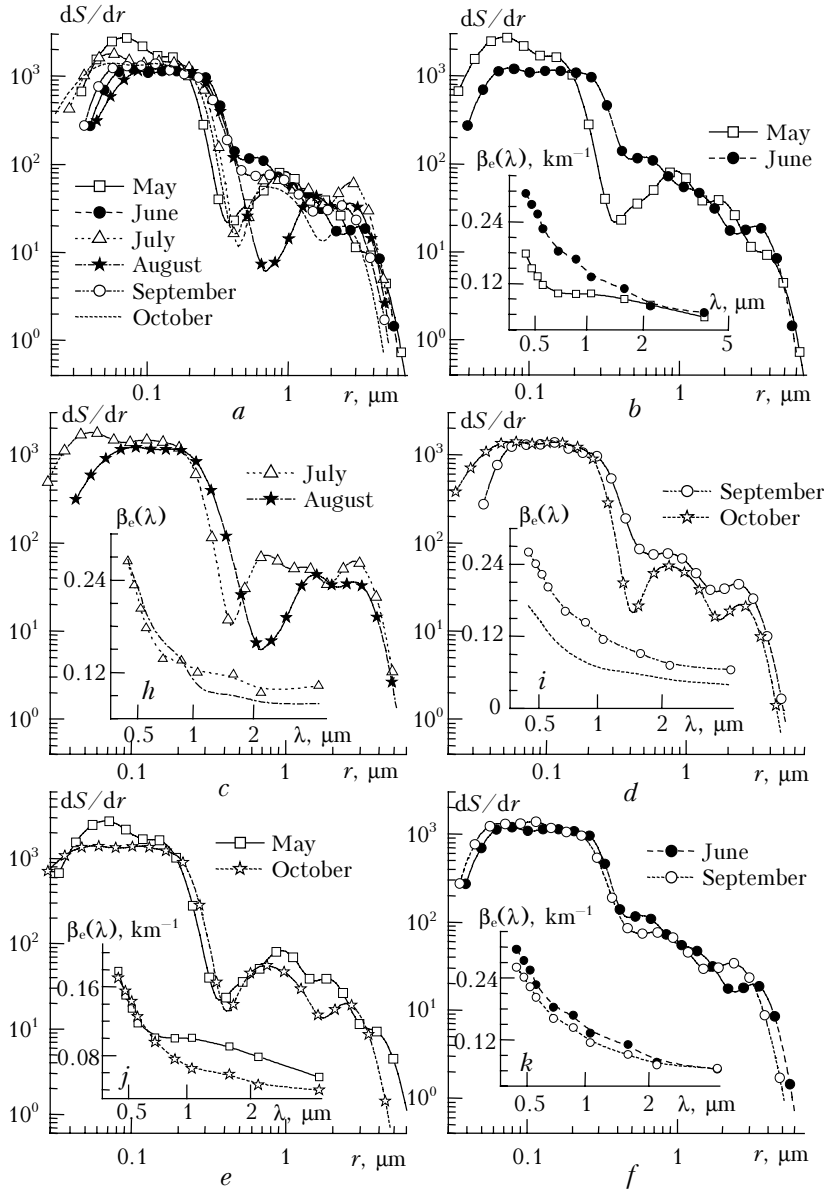

Fig. 13. Results of modeling the statistical variability: size spectra of the near-ground haze (*a–f*); mean spectral dependences $\overline{\beta_\varepsilon(\lambda)}$ measured at different stages of the experiment (*g–k*).

In particular, analysis based on the model estimates of the statistical variability of the empirical data on $\beta_\varepsilon(\lambda)$ obtained from the data of measurements in May and October (Figs. 13*a–c*) has revealed the enhanced content of fine aerosol with the particle radius $r < 0.1$ μm.

Obviously, the lower monthly mean values of temperature in the near-ground atmospheric layer and short duration of the sunshine in these seasons provided for the optimal conditions for survival of particles of the microdisperse (MD) aerosol fraction near the sources of emission and the underlying surface. As a rule, by virtue of the above noted peculiarities, weak dynamics of the daytime increase of the height of the mixing layer and low intensity of the convective air fluxes are observed in the mid-latitudes in May and October. It favors for the higher level of MD content in the near-ground, as is seen in the results of numerical modeling for the case of near-ground measurement paths (Figs. 13*a*, *b*).

The modeling performed show that the variability of the size spectrum of the accumulative fraction at the right-hand side boundary, which is displaced from 0.3 to 0.55 μm in summer, is important for the formation of the $\beta_\varepsilon^{(i)}(\lambda)$ spectrum in visible and near IR ranges. As monthly mean temperature increases in summer, the processes of "cold" and "hot" emission of microdisperse aerosols and aerosol producing substances, including water vapor, become more active. In this connection, the efficiency of forming the particles of the intermediate size range increases. In particular, the shift of the right-hand side boundary can occur both due to coagulation growth of the particles under anomalous accumulation of MD

fraction and due to condensation of water vapor in the atmospheric regions with the enhanced relative humidity ($q > 65\%$).

Laboratory investigations of the mechanism of formation of smoke aerosols[15] show that when the smoke mixture has passed through air mass with enhanced relative humidity, the water fraction of aerosol particles is formed, namely in the intermediate size ($r \sim 0.5$–0.75 μm). High values of the relative humidity at night observed in June and July due to radiative cooling of the near-ground layer ($q > 70\%$) led to a significant change in the size spectrum of haze, including a noticeable shift of the right-hand side boundary of the accumulative fraction (see curve *2* in Fig. 13*b*).

The important factor disturbing the characteristic size spectrum of the near-ground haze is the long-time presence of air masses enriched with smoke aerosols in the region. The data illustrating the dynamics of the aerosol extinction coefficient $\beta_\varepsilon(\lambda_i)$ at three wavelengths ($\lambda = 0.44$; 0.69; 3.9 μm) in June are shown in Fig. 14*a*. Analysis of the data shown in this figure shows that, since June 10 and until the end of month, variations of the parameters $\beta_\varepsilon(0.44)$ and $\beta_\varepsilon(0.69)$ are often more than twice as high as their mean values observed in May and October and well correlate with each other. At the same time, the dynamics of $\beta_\varepsilon(3.9)$ variations significantly differs from the rhythms of variations of two first parameters. Comparison of the model spectra dS/dr obtained in June and September (Fig. 13*f*) shows closeness of the spectra shapes and the relative proportions in the content of the fractions. The problem of the characteristic peculiarities of variations of the disperse composition of the near-ground haze in September was discussed in detail in Ref. 16, where it was shown that repeated intrusions of the air masses enriched with smokes were observed to this region in the fall. In particular, according to data shown in Fig. 14*b*, in September 2–8, the air mass (AM) with the most dense smokes has come (maximum of the optical density was observed on September 6 and was $\beta_\varepsilon(0.44) \approx 1.0$ km^{-1}).

Two episodes of the AM enriched with the smokes coming to the region of measurements were observed in September (from 10 to 14 and from 18 to 23) (see Figs. 14*b* and *c*). Intrusion of an extremely clean Arctic AM was observed between the second and third episodes on September 14. The extremely rare situation of anomalous spectral behavior of the coefficient $\beta_\varepsilon(\lambda_i)$ was observed on this day in the near-ground atmospheric layer. Taking into account the above peculiarities of the data acquired, some reasons appear to suppose that smoke aerosols noticeably affect the variability of data on $\beta_\varepsilon(\lambda_i)$ spectra both in June and September.

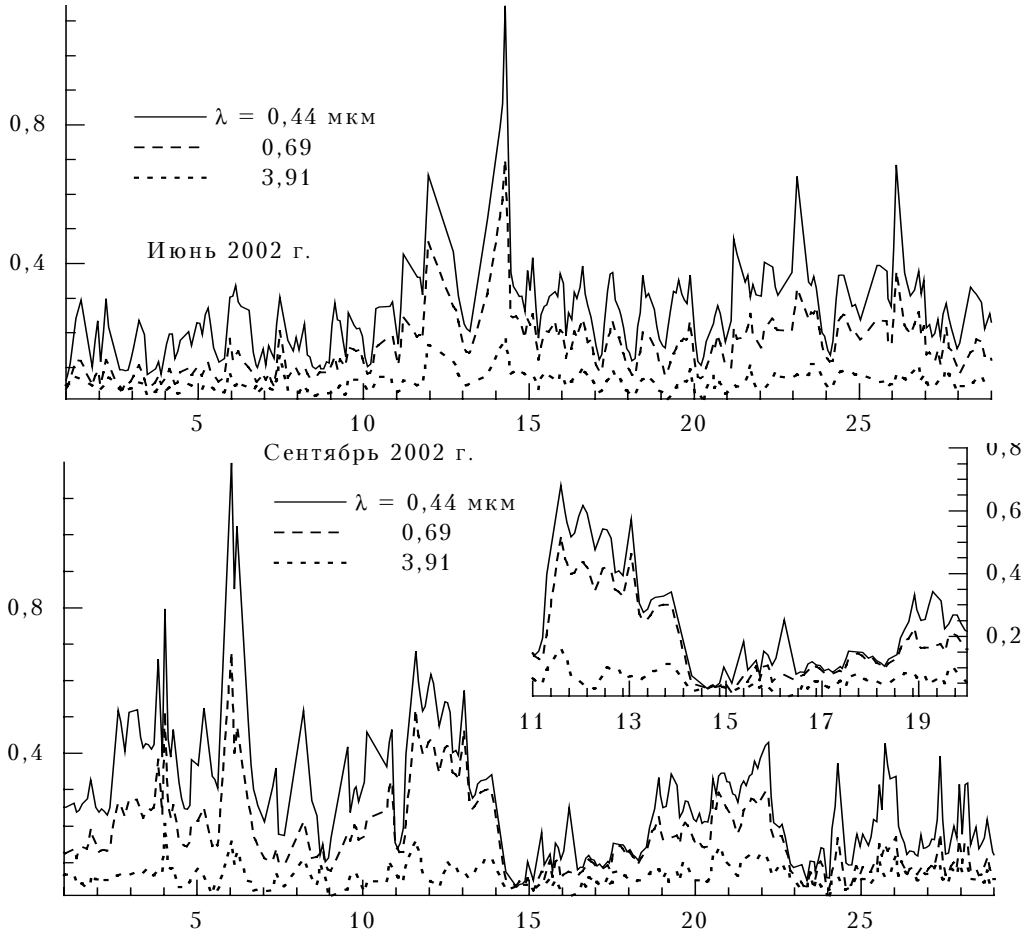

Fig. 14. Time variability of the spectral aerosol extinction coefficient $\beta_\varepsilon(\lambda_i)$ at three wavelengths $\lambda = 0.44$, 0.69, 3.9 μm in June (*a*) and in September 2002 (*b* and *c*).

One should emphasize that sporadically appeared episodes on intensification of emission of fine aerosols and the compounds forming them during forest and peatbog fires make the study of seasonal features of the variability of the haze particle size spectrum essentially more difficult. In our opinion, this fact causes the revealed instability of the near-ground haze particle size spectrum in the intermediately dispersed range (see Fig. 13*a*). As shown in Ref. 16, variations of the velocity of the AM motion, trajectory of propagation of smokes inside the AM, and the distance of the sources of burning from the region of measurements are important in interpreting the mechanism of formation of the aerosol disperse composition in this size range.

The behavior of the size spectra of the haze dS/dr in the size range of the coarse fraction (Figs. 13*a–f*) confirms the conclusions drawn earlier (Figs. 10–12 and Tables 5–6) on the important role of the convective emission of the coarse aerosol in summer.

The spectra characterizing the microphysical variations of the near-ground haze in May and June are shown for a comparison in Figs. 13*b* and *g*. In spite of approximately equal total cross section of the particles of the accumulative fraction ($\overline{S}_{123} \sim 16.6\ \mu m^2 \cdot cm^{-3}$ in May and $20.0\ \mu m^2 \cdot cm^{-3}$ in June) and coarse particles ($\overline{S}_{456} \sim 74.1\ \mu m^2 \cdot cm^{-3}$ in May and $85.2\ \mu m^2 \cdot cm^{-3}$ in June), essential differences in the measured spectral dependences $\beta_\varepsilon(\lambda_i)$ are observed (Fig. 13*g*). As is easily seen (Figs. 13*b* and *g*), significant increase of the parameter $\beta_\varepsilon(\lambda_i)$ in the short-wave range in June is caused by a significant shift of the right-hand side boundary of the accumulative fraction toward the intermediate size range, and all this takes place in spite of the enhanced content of the fine fraction in May.

The decrease of the optical effect of large particles is observed when passing from July to August (Figs. 13*c* and *h*), that agrees with the decrease of monthly mean air temperature near the underlying surface in August and the decrease of the efficiency of convective filling of the layer with the coarse aerosols. Let us note that the values $\overline{\beta_\varepsilon(\lambda)}$ in the visible wavelength range in July and August are practically equal to each other.

The comparison of data obtained in September and October (Figs. 13*d* and *i*) shows that the sharp decrease of the content of large particles with $r > 0.6$ μm as the cold season approaches and heating of the underlying surface weakens predetermines the decrease of $\overline{\beta_\varepsilon(\lambda)}$ in the entire spectral range studied.

The functions dS/dr for May and October are shown in Fig. 13*e* and the corresponding monthly mean spectral dependences of the extinction coefficient $\beta_\varepsilon(\lambda)$ are shown in Fig. 13*j*. In spite of the closeness of the spectral behavior $\beta_\varepsilon(\lambda)$ in the visible range, the differences taking place in the IR range are caused by the enhanced content of the coarse fraction in May. Obviously, the latter is related to higher air temperatures in the near-ground layer in May (see Fig. 3*b*).

Conclusions

Summarizing the results presented, one can recognize that the peculiarities of the disperse composition of the near-ground haze at different stages of the experiment appeared due to the characteristic changes in the content of particles in three subranges of the size spectrum, namely, accumulative ($r < 0.45$ μm), intermediate ($0.45 < r < 2.0$ μm), and the coarse ($r > 2.2$ μm) fractions. The particle-volume size distribution of the accumulative fraction shows quite sharp right-hand boundary. At the same time, the spectrum in the intermediate size range, up to 0.8 μm from the left, is being filled in only sporadically and has the dynamics of variations different from that characteristic of the neighbor range ($r > 0.8$ μm), which more often coincides with the activity of the sources of thermal emission of aerosols (forest fires, peatbog smoldering). The right-hand side boundary of the intermediate size range ($0.8 < r < 2.0$ μm) shows related dynamics with particles of the coarse fraction, agreeing with activating the thermal component of the turbulent mixing. This conclusion is especially well confirmed by the example of the spectrum reconstructed using the data acquired in July.

Relatively high correlation of the values $\beta_\varepsilon(\lambda)$ in the visible range with the content of different aerosol fractions is an evidence of the fact that the size spectrum of the near-ground haze shows correlated changes. As a consequence, correlated variations of the fraction composition of the near-ground haze in short time intervals are an evidence of the important role of stable (diurnal) variations of meteorological parameters in the change of the optical and microphysical state of aerosol near the underlying surface.

Stable deformations of the size spectra of the accumulative aerosol fraction under the effect of the relative air humidity, as well as diurnal variations of the mean content of coarse aerosol related to the change of the turbulent mixing regime are the main causes of the correlated changes in the size spectrum of the near-ground haze as a whole.

The estimates obtained show that the values $\beta_\varepsilon(\lambda)$ at the wavelengths $\lambda > 0.8$ μm are mainly governed by the dynamics of the content of the intermediate and coarse aerosol fractions. All the three fractions play certain roles in the formation of the spectral variability of $\beta_\varepsilon(\lambda)$ in the visible range.

One should also recognize that some of the peculiarities noted in the change of the disperse composition of the near-ground haze, in passing from one month to another, are not universal, but only reflect the peculiarities of its formation only in the season of the considered year. We plan further investigation of them based on conducting analogous measurements in the future experiments.

Acknowledgments

The work was supported in part by Russian Foundation for Basic Research (grant No. 01-05-65197).

References

1. G.V. Rosenberg, G.I. Gorchakov, Yu.S. Georgievskii, and Yu.S. Lyubovtseva, in: *Atmospheric Physics and Problems of Climate* (Nauka, Moscow, 1980), pp. 216–257.
2. V.L. Filippov, A.S. Makarov, and V.P. Ivanov, Dokl. Akad. Nauk SSSR **265**, No. 6, 216–257 (1982).
3. G.M. Krekov and R.F. Rakhimov, *Optical-Radar Model of Continental Aerosol* (Nauka, Novosibirsk, 1982), 200 pp.
4. N.N. Paramonova, A.M. Brounshtein, and V.I. Privalov, Trudy Gl. Geofiz. Obs., No. 496, 84–93 (1985).
5. M.V. Kabanov, M.V. Panchenko, Yu.A. Pkhalagov, et al., *Optical Properties of Coastal Atmospheric Hazes* (Nauka, Novosibirsk, 1988), 202 pp.
6. Yu.A. Pkhalagov, V.N. Uzhegov, and N.N. Shchelkanov, Atmos. Oceanic Opt. **9**, No. 7, 598–602 (1996).
7. R.F. Rakhimov and M.V. Panchenko, Atmos. Oceanic Opt. **12**, No. 2, 103–114 (1999).
8. Yu.A. Pkhalagov, V.N. Uzhegov, and N.N. Shchelkanov, Atmos. Oceanic Opt. **5**, No. 6, 423–426 (1992).
9. Yu.A. Pkhalagov and V.N. Uzhegov, Opt. Atm. **1**, No. 10, 3–11 (1988).
10. A.M. Obukhov, Izv. Akad. Nauk SSSR, Geofiz., No. 3, 432–439 (1960).
11. I.E. Naats, *Theory of Multi-Frequency Laser Sounding of the Atmosphere* (Nauka, Novosibirsk, 1980), 157 pp.
12. V.E. Zuev and G.M. Krekov, *Optical Models of the Atmosphere* (Gidrometeoizdat, Leningrad, 1986), 256 pp.
13. A.A. Semenov, *Theory of Electromagnetic Waves* (Moscow State University Publishing House, Moscow, 1968), 318 pp.
14. E.V. Makienko, R.F. Rakhimov, S.M. Sakerin, and D.M. Kabanov, Atmos. Oceanic Opt. **15**, No. 7, 531–540 (2002).
15. R.F. Rakhimov, V.S. Kozlov, M.V. Panchenko, A.G. Tumakov, and V.P. Shmargunov, Atmos. Oceanic Opt. **14**, No. 8, 624–628 (2001).
16. E.V. Makienko, R.F. Rakhimov, V.N. Uzhegov, and Yu.A. Pkhalagov, Atmos. Oceanic Opt. **16**, No. 12, 1008–1012 (2003).